


Extreme pulse generation by an interband cascade laser with optical injection and step-down current perturbations

Y. Mao  and W. Feng**School of Physics and Electronic Engineering, Jiangsu University, 301 Xuefu Road, Zhenjiang, Jiangsu Province 212013, China*G. H. Song , C. Wang ,[†] and J. C. Cao*Center of Materials Science and Optoelectronics Engineering, University of Chinese Academy of Sciences, Beijing 100049, China and State Key Laboratory of Materials for Integrated Circuits, Shanghai Institute of Microsystem and Information Technology, Chinese Academy of Sciences, 865 Changning Road, Shanghai 200050, China*

(Received 2 August 2023; revised 3 November 2023; accepted 11 April 2024; published 6 May 2024)

The dynamic performance of an interband cascade laser (ICL) with optical injection is studied within the framework of rate equations. The effect of stage number m and active area A on the ICL optical injection-locking diagram is numerically simulated. ICLs with a small stage number and large active area have a relatively large phase-locked region. When the stage number is small, the system exhibits a large number of extreme pulses in the frequency-unlocked region. We show that step-down perturbations of the laser pump current can trigger and suppress extreme pulses by changing the parameters of amplitude, duration, and modulation time points. The amplitude and duration of current perturbation have a significant impact on the number of extreme pulses. This work provides different insight into the generation and control of extreme pulses based on ICLs.

DOI: [10.1103/PhysRevA.109.053506](https://doi.org/10.1103/PhysRevA.109.053506)

I. INTRODUCTION

Interband cascade lasers (ICLs) are one of the important laser sources in the midinfrared spectral range [1]. The emission wavelength of the ICL is determined by its interband energy difference, and each injected electron generates multiple photons through several stages connected in series. Its series connection ensures that carriers are injected uniformly in each active region, resulting in a lower carrier concentration required for threshold than in conventional diode lasers. This reduces optical and Auger losses and lowers the threshold current density. Conventional bipolar diode lasers require both n -type and p -type cladding regions. p -type layers tend to absorb more light than n -type layers, leading to higher losses. ICLs just need an n -type cladding, inserted at either end of the cascade stages to transfer electrons in and out. Therefore, ICLs are characterized by low threshold current density and high quantum efficiency [2,3]. ICLs have the same scheme of carrier cascading as quantum cascade lasers (QCLs), while the electronic transition in ICLs occurs between the conduction band and valence band [4,5]. ICLs usually operate in the 3–6 μm band, while QCLs display good performance in the 4–13 μm . Compared with QCLs, ICLs have lower power consumption, typically, 1 or 2 orders of magnitude lower than QCLs [6]. ICLs were used in NASA's Mars Curiosity rover for methane gas detection on Mars [7], indicating their promising application prospects.

An ICL is a class-B laser with carrier lifetime in the nanosecond range. When external perturbation is applied, the class-B laser system will become unstable due to the additional degrees of freedom [8]. The chaotic behavior of class-B lasers can be observed by adding external modulation of laser parameters, optical injection, and optical feedback [9–16]. Using the self-mixing interferometry technique, Deng *et al.* measured above-threshold linewidth enhancement factors of ICLs as about 2.2, which did not change with increasing pump current [17]. Subsequently, they proposed an ICL rate-equation model for the study of modulation dynamics and optical noise characteristics [18]. Han *et al.* conducted a theoretical study on the nonlinear dynamics of ICL subjected to optical feedback [19]. Their results showed that an ICL with few stage numbers subjected to external cavity optical feedback is more susceptible to exhibiting chaos.

Despite the rapid progress in fundamental science and applications based on ICLs, some key issues of laser dynamics remain unsolved. One of the unsolved problems is the extreme optical pulse generation in ICLs under optical injection. The study of the dynamics of ICLs under optical injection is still in its early stages, and no studies have been reported in the literature. We speculate that the laser injection efficiency of the master laser is very low, making it difficult to control the slave laser experimentally. An ICL with optical injection provides a good test bed for studying extreme pulses. Optical extreme pulses are also called optical rogue waves (RWs) [20], and the probability distribution function (PDF) of their intensity values has the qualitative characteristic of a long tail. Extreme pulses have become a hot topic in the field of semiconductor lasers, attracting much attention [21]. Bonatto *et al.* demonstrated extreme pulses in a semiconductor laser with

*wfeng@ujs.edu.cn

[†]cwang@mail.sim.ac.cn

optical injection for the first time [22]. They defined criteria for RWs, whose threshold value is $\mu + 8 \times \sigma$ (with σ being the standard deviation and μ being the mean), that are now widely used to describe extreme events in nonlinear systems. They also showed the emergence of superextreme events in a CO₂ laser system. The amplitude deviation is well above the $4 \times \sigma$ ($8 \times \sigma$) criterion, and regular patterns are found in the time series of laser intensities. The regular patterns can predict the occurrence of extreme events, linked to unstable periodic orbits embedded in chaotic attractors that can control the laser dynamics [15]. Zamora-Munt *et al.* demonstrated that the mechanism generating extreme pulses is an external crisislike process in the form of an attractor generated from a crossing of the attractor generated from one fixed point with the stable manifold of another fixed point [23]. Spitz *et al.* observed extreme pulses in a midinfrared QCLs with optical feedback and found that small-amplitude cyclic modulation of the pump current could generate extreme pulses with high success [24]. Tian *et al.* investigated the effect of step-up current perturbations on extreme pulses under different parameters. They found that as an extreme pulse begins, the phase grows abruptly and reaches a local maximum at the peak of the pulse. Then, when the pulse is over, the phase falls to a value which is similar to the one before the pulse started [25].

On-demand generation of ultrahigh-intensity optical pulses can broaden the applications of ICLs for imaging and sensing. For example, controlled generation of pulses with ultrahigh peak time intensities can reduce the signal-to-noise ratio to improve image quality. In this paper we study the dynamic property of ICLs with optical injection and propose a method for controlling extreme pulses by applying step-down current perturbations. The remainder of this paper is organized as follows. In Sec. II, we describe the semiclassical rate-equation model for the ICL system with optical injection. In Sec. III, the dynamic characteristics of the ICL under optical injection are studied. We numerically investigate the effect of important parameters, such as the stage number and active area, on the optical injection-locking diagram of ICLs. In the negative-frequency-detuning part of the frequency-unlocked region, the ICL displays extreme pulses. We show that step-down perturbations of the pump current can trigger or suppress such extreme pulses. We also study the effects of

the modulation amplitude, modulation duration, and modulation time point on such extreme pulses. Finally, in Sec. IV, we draw the main conclusions of the work.

II. RATE EQUATIONS FOR AN ICL SUBJECTED TO OPTICAL INJECTION

Based on the rate-equation modeling of ICLs in Ref. [18] and the classical injection-locking model developed in Ref. [26], the rate equations for an ICL with optical injection are expressed as follows:

$$\frac{dN(t)}{dt} = \eta \frac{I_0}{q} - \Gamma_p v_g g S(t) - \frac{N(t)}{\tau_{sp}} - \frac{N(t)}{\tau_{aug}}, \quad (1)$$

$$\frac{dS(t)}{dt} = \left[m \Gamma_p v_g g - \frac{1}{\tau_p} \right] S(t) + m \beta \frac{N(t)}{\tau_{sp}} + 2k_c \sqrt{S_{inj} S(t)} \cos \phi(t), \quad (2)$$

$$\frac{d\phi(t)}{dt} = \frac{\alpha}{2} \left[m \Gamma_p v_g g - \frac{1}{\tau_p} \right] - k_c \sqrt{\frac{S_{inj}}{S(t)}} \sin \phi(t) - 2\pi F_{inj}. \quad (3)$$

Here, $N(t)$ is the carrier number per stage, $S(t)$ is total photon number of all gain stages, and $\phi(t)$ is the phase of the electric field. S_{inj} is the photon number of the master laser, and the injection ratio is defined as $R_{inj} = S_{inj}/S_0$, with S_0 being the photon number of the free-running laser. S_0 can be obtained by solving the steady state of the free-running ICL, i.e., $S_0 = m \eta \tau_p (I - I_{th})/q$. I_{th} is the threshold current [18]. F_{inj} is the frequency detuning, defined as the lasing frequency difference between the master laser and the slave laser. k_c is the coupling coefficient of the two lasers, $k_c = v_g(1 - R)/(2L\sqrt{R})$, with v_g being the light group velocity, L being the laser cavity length, and R being the facet reflectivity [27]. g , the material gain per stage, is given by $g = a_0[N(t) - N_{tr}]/A$, with a_0 being a different gain, N_{tr} being the transparent carrier number, and A being the active area. Other parameters can be found in Table I. We solve the rate equations using the fourth-order Runge-Kutta method. The integration time step is 1 ps. We solve the steady-state solution for an ICL operating above the threshold current [19] and obtain the dependence of the

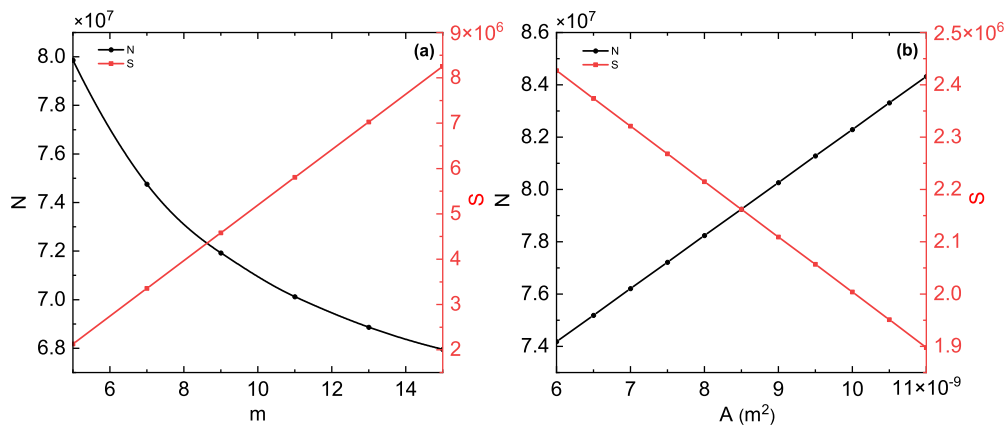


FIG. 1. (a) Carrier number and photon number vs stage number. The other parameter is $A = 8.8 \times 10^{-9} \text{ m}^2$. (b) Carrier number and photon number vs active area. The other parameter is $m = 5$.

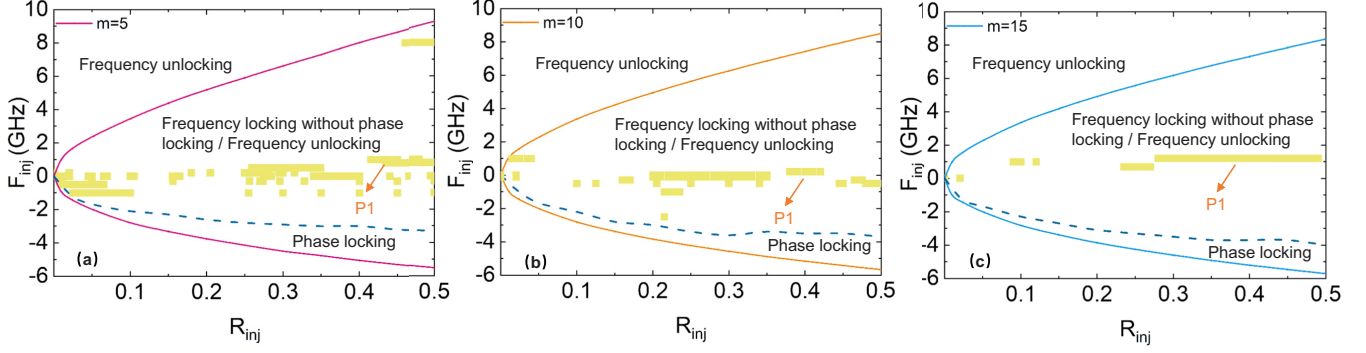


FIG. 2. Optical injection-locking diagram drawn by plotting the detuning frequency vs the injection ratio with stage numbers (a) $m = 5$, (b) $m = 10$, and (c) $m = 15$. Above the dashed line and below the solid line is the frequency-locked region without phase locking or frequency-unlocked region. Below the dashed line and above the solid line is the phase-locked region. Beyond the solid line is the frequency-unlocked region. The yellow parts show P1 oscillations. The active area is $A = 8.8 \times 10^{-9} \text{ m}^2$.

carrier number and photon number on the stage number and active-region area when the bias current is 0.03, as shown in Figs. 1(a) and 1(b), respectively. The larger the stage number m is, the larger the photon number is, and the smaller the carrier number is. The larger the active area A is, the smaller the photon number is, and the larger the carrier number is. In the simulations in this paper, we mainly focus on the effect of current perturbations on the system.

III. DYNAMICS BEHAVIORS OF AN ICL SUBJECTED TO OPTICAL INJECTION

A. Locking map of the ICL

Neglecting the spontaneous term in Eq. (2) and setting the left-hand sides of rate equations (1)–(3) to zero, the steady-state solution with optical injection is obtained as follows:

$$S = \frac{4k_c^2 S_{\text{inj}}}{(m\Gamma_p v_{gg} - 1/\tau_p)^2 + [\alpha(m\Gamma_p v_{gg} - 1/\tau_p) - 4\pi F_{\text{inj}}]^2}, \quad (4)$$

$$N = \frac{[\eta \frac{I_0}{q} - \Gamma_p v_{gg} S](\tau_{\text{sp}} + \tau_{\text{aug}})}{\tau_{\text{sp}} \tau_{\text{aug}}}, \quad (5)$$

$$\phi = \sin^{-1} \left[\frac{2\pi F_{\text{inj}}}{k_c \sqrt{1 + \alpha^2}} \sqrt{\frac{S}{S_{\text{inj}}}} \right] - \tan^{-1} \alpha. \quad (6)$$

First, we consider the injection-locking map of the ICL. The boundaries derived from Eqs. (5) and (6) show that the variation of the phase across the locking range varies from $\cot^{-1} \alpha$ at the negative-frequency-detuning edge to $-\pi/2$ at the positive-frequency-detuning edge. Then, the locking regime can be obtained by rearranging Eq. (6):

$$F_{\text{inj}} = \frac{-k_c \sqrt{1 + \alpha^2} \sqrt{S_{\text{inj}}/S} \sin[\phi + \tan^{-1} \alpha]}{2\pi}. \quad (7)$$

The above calculation method for the locking range of the ICL is the same as the method used in Ref. [33] for the locking range of a Mid-infrared QCL with optical injection. Thus, both types of lasers have the same expression for the locking range (7).

Figure 2 shows injection-locking diagrams drawn by plotting the detuning frequency F_{inj} vs the injection ratio R_{inj} for different stage numbers m . The boundaries (solid line) are obtained from Eqs. (5), (6), and (7). In the phase-locked region, the difference in phase between the master and slave

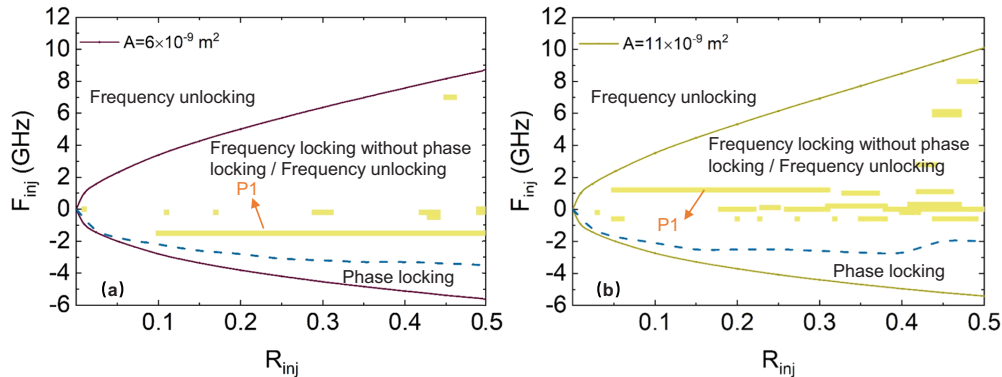


FIG. 3. Optical injection-locking diagram drawn by plotting the detuning frequency vs the injection ratio with (a) $A = 6 \times 10^{-9} \text{ m}^2$ and (b) $11 \times 10^{-9} \text{ m}^2$. Above the dashed line and below the solid line is the frequency-locked region without phase locking or frequency-unlocked region. Below the dashed line and above the solid line is the phase-locked region. Beyond the solid line is the frequency-unlocked region. The yellow parts show P1 oscillations. The stage number is $m = 5$.

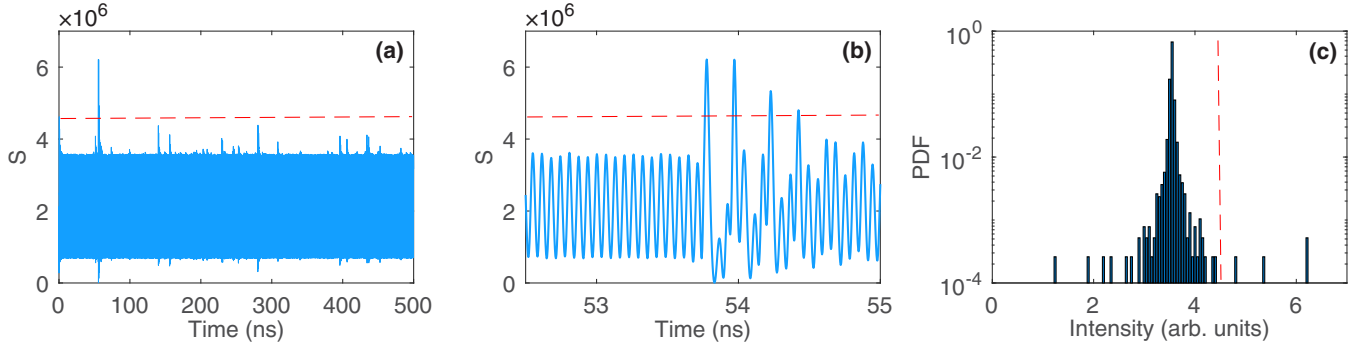


FIG. 4. (a) Time series that exhibit extreme intensity pulses for $R_{\text{inj}} = 0.4$ and $F_{\text{inj}} = -7.5$ GHz. (b) Magnified diagram of the extreme pulses in (a). (c) The histogram associated with (a). The other parameters are $m = 5$ and $A = 8.8 \times 10^{-9} \text{ m}^2$.

lasers is constant, and the dynamic variables describing the system reach a constant value. The dashed line is the boundary of the phase-locked region. In the frequency-locked region without phase locking, the difference in phase changes in time but remains bounded. In the frequency-unlocked region, the difference in phase increases or decreases unboundedly [34]. As shown in the Fig. 2, as the stage number m increases, the phase-locked region becomes narrower. In the part below the solid line and above the dashed line, there are periodic and nonperiodic oscillations distributed. Some are frequency-locked solutions without phase locking and some are frequency-unlocked solutions. Period-1 (P1) oscillations gather in the narrowing -1 to 1 GHz range. The dynamical state is complex in this region. Solutions outside the boundary of the solid line are all frequency unlocked. The stage number m has effects on the photon number and the optical phase. An increase in m leads to an increasing photon number, which promotes fluctuations in the optical phase and narrows the phase-locked region. Figure 3 shows injection-locking diagrams drawn by plotting the detuning frequency F_{inj} vs the injection ratio R_{inj} for different active areas A . It is observed that as the active area A increases, the phase-locked region increases, and the range of P1 oscillations increases.

Therefore, in ICLs, a small stage number and large active area lead to a large phase-locked region and more P1 oscillations. P1 oscillations provide attractive candidates for the generation of high-quality midinfrared photonic microwaves [35].

B. Optical extreme pulse generation in ICLs

In the frequency-unlocked region outside the solid line, there are time series that behave as series of small pulses and sporadic extreme intensity pulses, as shown in Fig. 4(a). We use the judgment criteria of $\mu + 8\sigma$ (with σ being the standard deviation and μ being the mean). Each time we calculate a time interval of 500 ns. We drop the previous transient process and calculate the threshold to be 4.4. The red dashed line shows the RW threshold. Figure 4(b) shows a magnified diagram of the extreme pulses, and there are four extreme pulses above the threshold. To confirm that it has RW characteristics, a histogram of the peak laser intensity is plotted. Figure 4(c) clearly shows the tail is longer than the RW thresholds, indicating the presence of extreme pulses in this time series.

Figure 5 shows the number of extreme pulses in the frequency-unlocked region for $m = 5, 10,$ and 15 . There are few extreme pulses in the large detuned frequency region, so we start with $F_{\text{inj}} = -6$ GHz. When $m = 5$, there are extreme pulses in a large area of the diagram. From -8 to -10 GHz, the extreme pulses are widely distributed and numerous. When $m = 10$, the region where extreme pulses exist is greatly reduced. They are also concentrated from -8 to -10 GHz. When $m = 15$, extreme pulses exist only in a small region. The number of extreme pulses occurring in the frequency-unlocked region shows an overall decreasing trend as m increases. And the area where extreme pulses occur decreases. Reference [22] showed that RWs can be excited

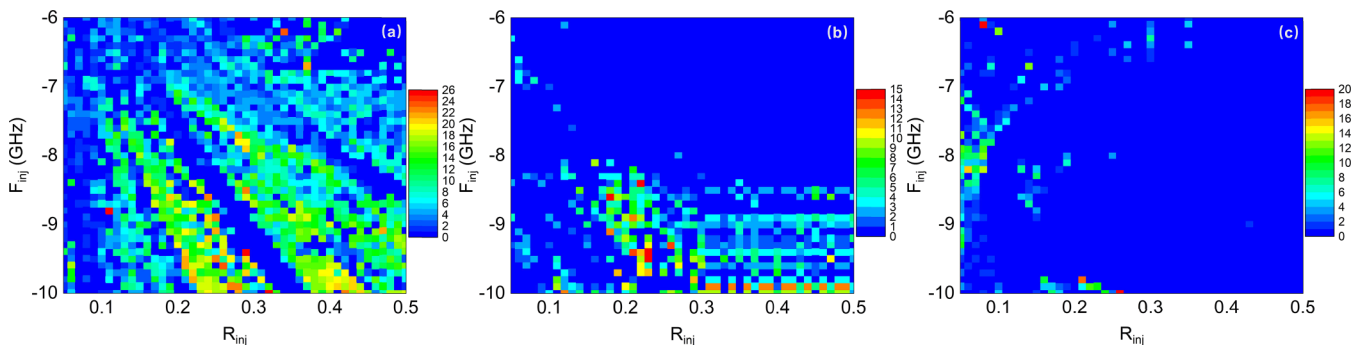


FIG. 5. Number of generated extreme pulses as a function of injection ratio R_{inj} and detuning frequency F_{inj} for (a) $m = 5$, (b) 10 , and (c) 15 . The active area is $A = 8.8 \times 10^{-9} \text{ m}^2$.

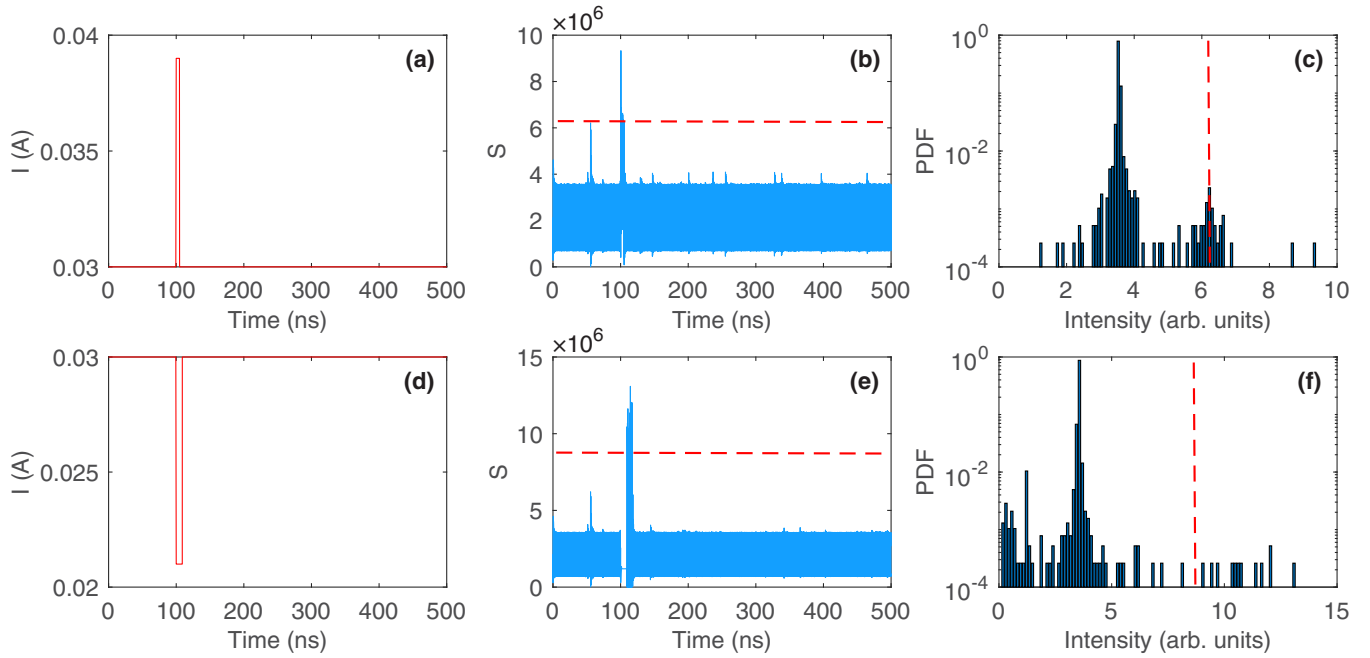


FIG. 6. (a) Example of pump-current step-up perturbation, (b) the generated pulses, and (c) the histogram associated with it. The step-up current is 0.039 A, and its duration is 5 ns. (d) Example of pump-current step-down perturbation, (e) the generated pulses, and (f) the histogram associated with it. The step-down current is 0.021 A, and its duration is 9 ns. The other parameters are $m = 5$ and $A = 8.8 \times 10^{-9} \text{ m}^2$.

only if the carrier density is sufficiently high. Therefore, we think that large numbers of stages reduce the carrier density and fail to meet the requirements for exciting extreme pulses.

With the parameter conditions in Fig. 4, we exert a step-up current perturbation as shown in Fig. 6(a) on the ICL system, which produces the extreme pulses depicted in Fig. 6(b). Figure 6(c) shows the PDF associated with it. Extreme pulses can be emitted due to the sudden increase in carrier density caused by the step-up perturbation of the pumping current. This situation has been studied in semiconductor lasers [25]. In this section we focus our work on the excitation of extreme pulses by step-down current perturbation [shown in Fig. 6(d)]. Figure 6(e) shows that the step-down current perturbation can also generate extreme pulses. Figure 6(f) shows the PDF associated with it. The pump current drops abruptly, experiences a period of modulation, and then suddenly rises to its original level. The step-down current disturbance abruptly decreases the carrier density, which is followed by an abrupt increasing of the carrier density after a period of time, which excites extreme pulses. The extreme pulses generated by the step-up current perturbation occur during the step-up process, while the extreme pulses generated by the step-down current perturbation occur after the step-down process.

In order to analyze the effect of step-down current perturbation with different laser parameters, we inject a pump current into the laser system as shown in Fig. 6(d). A mapping graph is plotted in Fig. 7. We apply the perturbation only once in the time interval of 0–500 ns. In comparison to Fig. 5(a), in the presence of current perturbation, some extreme pulses appear in a part of the parameter region where no extreme pulses occurred before. Most of the parameter region (–8 to –10 GHz) where extreme pulses were present is, instead, suppressed because the current modulation causes more high

pulses in this parameter region, resulting in an increase in the threshold for extreme pulses. High pulses are those close to the threshold but below it, while extreme pulses are those above the threshold. There is also a part of the parameter region where extreme pulses fail to be excited. We speculate that the reason is that the pump-current perturbation failed to make the carrier density reach a high enough value to emit extreme pulses.

Two sets of parameters are selected from the region where no extreme pulses existed originally, and the effects of modulation duration and amplitude on the number of extreme pulses are investigated. The results are presented in Fig. 8. Figure 8 displays the number of pulses in the plane defined by (step-down current I , duration D) when the laser parameters

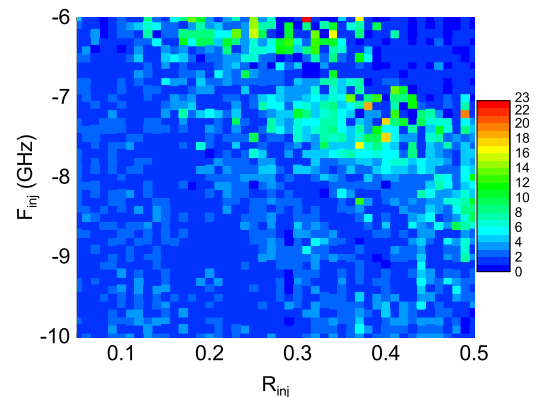


FIG. 7. Number of generated extreme pulses as a function of the injection ratio R_{inj} and detuning frequency F_{inj} . The step-down current is 0.021 A, and its duration is 9 ns. The other parameters are $m = 5$ and $A = 8.8 \times 10^{-9} \text{ m}^2$.

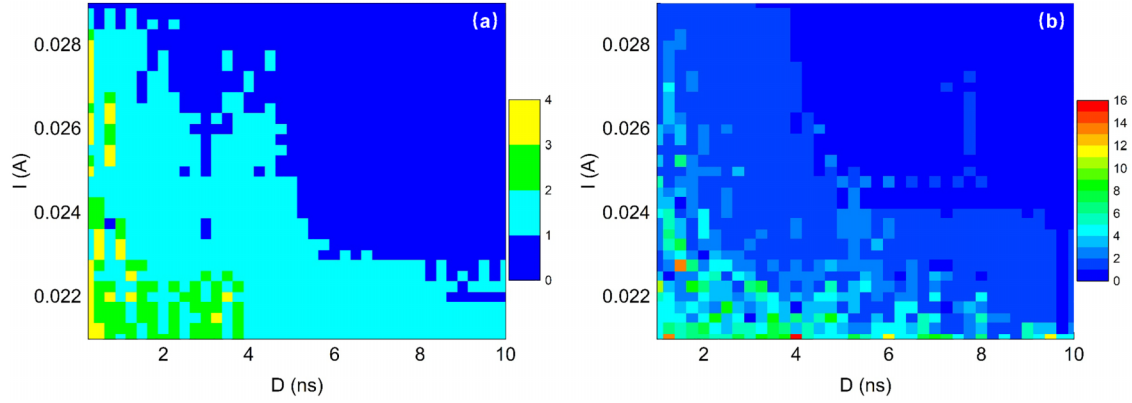


FIG. 8. Number of generated intensity pulses as a function of the step-down current I and the duration of modulation D . The parameters used are (a) $R_{inj} = 0.05$ and $F_{inj} = -7.6$ GHz and (b) $R_{inj} = 0.37$ and $F_{inj} = -7.6$ GHz. The other parameters are $m = 5$ and $A = 8.8 \times 10^{-9} \text{ m}^2$.

are $R_{inj} = 0.05$ and $F_{inj} = -7.6$ GHz [labeled A; Fig. 8(a)] and $R_{inj} = 0.37$ and $F_{inj} = -7.6$ GHz [labeled B; Fig. 8(b)]. The smaller current I in the vertical coordinate represents the larger modulation amplitude, and the perturbation modulation time is $t = 100$ ns. These two sets of parameters are perturbed with different success rates. We speculate that point A is located in a poor region that generates extreme pulses spontaneously, while point B is located in a rich region that generates extreme pulses spontaneously. So point B has a significantly higher probability of success than point A. We observe that large perturbation amplitudes benefit the extreme pulses produced. When the duration of the perturbation is longer, it may lead to an increased number of high pulses, which raises the threshold of extreme pulses. As a result, the number of extreme pulses decreases. In the other case, after a longer time perturbation, the high pulse cannot even be excited. When the perturbation amplitude is large enough ($I \approx 0.021$ A), the number of extreme pulses does not decrease to zero, even if the duration of the perturbation is long. This suggests that extreme pulses are unlikely to be triggered by short perturbations. If the perturbations are small, the duration must be very short.

To analyze whether the number of extreme pulses generated is related to the time point of the modulation, we fix the step-down current ($I = 0.021$ A) and vary the modulation time point and modulation duration. The time point of the modulation is the instant of time at which the modulation is applied. The results are shown in Fig. 9. From Fig. 9 we can see that the time point of the modulation produces no particular pattern for the change in the number of extreme pulses. By comparing Figs. 4(a), 6(b), and 6(e), it is observed that the pulse shapes and the intensity are the same in all three plots before the current perturbation is added. The reason is that we use the same initial values in the calculation. From the moment the perturbation is added, the pulses in the time series are no longer identical. The extreme pulses generated by either the step-down perturbation or the step-up perturbation are due to the perturbation applied locally in the time series. In a numerical calculation, we consider the value of the previous moment as the initial condition for the next moment. So the perturbation can be considered the initial condition of the next moment. The extreme pulses belong to chaotic dynamics behavior. The results obtained are complicated because chaos is extremely sensitive to the initial conditions. But that does

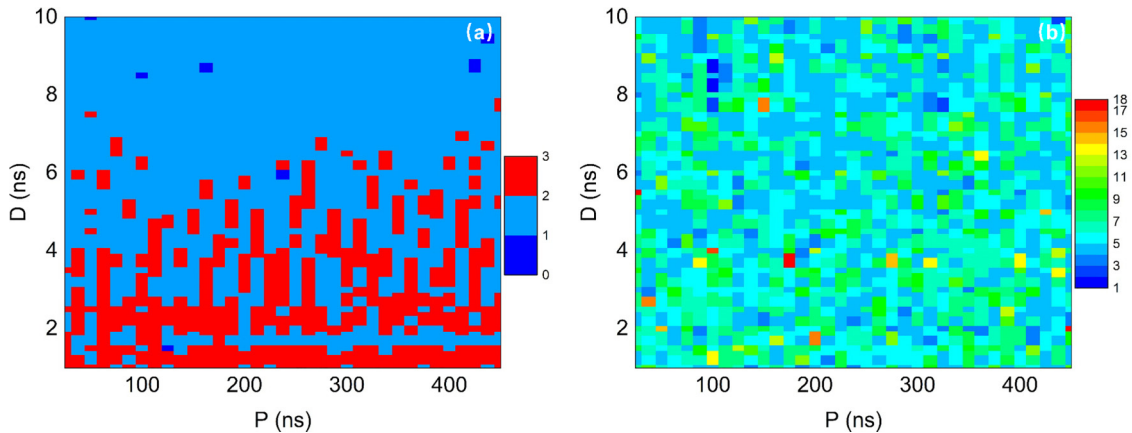


FIG. 9. Number of generated intensity pulses as a function of the duration of modulation D and the time point of modulation P . The parameters used are (a) $R_{inj} = 0.05$ and $F_{inj} = -7.6$ GHz and (b) $R_{inj} = 0.37$ and $F_{inj} = -7.6$ GHz. The other parameters are $m = 5$ and $A = 8.8 \times 10^{-9} \text{ m}^2$.

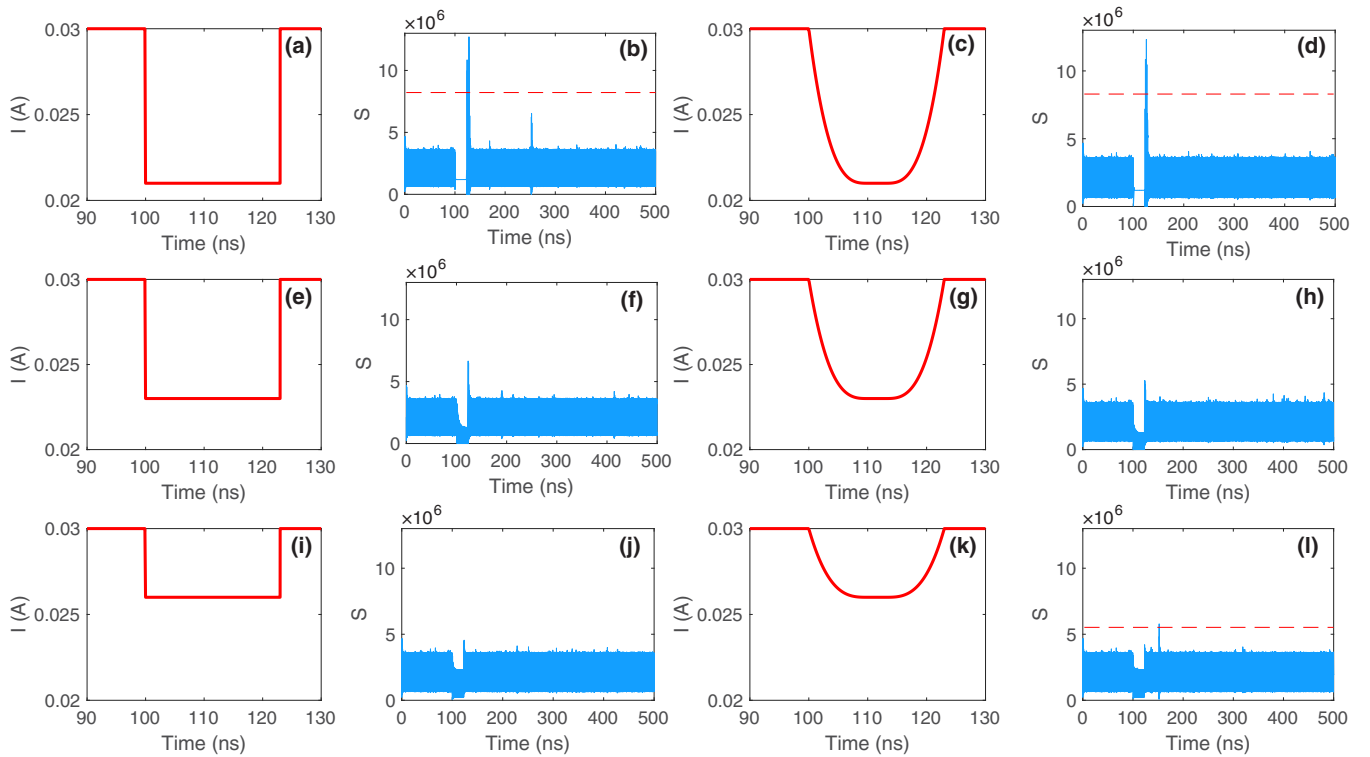


FIG. 10. (a) Abrupt pump-current perturbation from 0.03 to 0.021 A and (b) the resulting pulses. (c) Smooth pump-current perturbation from 0.03 to 0.021 A and (d) the resulting pulses. (e) Abrupt pump-current perturbation from 0.03 to 0.023 A and (f) the resulting pulses. (g) Smooth pump-current perturbation from 0.03 to 0.023 A and (h) the resulting pulses. (i) Abrupt pump-current perturbation from 0.03 to 0.026 A and (j) the resulting pulses. (k) Smooth pump-current perturbation from 0.03 to 0.026 A and (l) the resulting pulses. The other parameters are $R_{\text{inj}} = 0.4$, $F_{\text{inj}} = -7.3$ GHz, $m = 5$, and $A = 8.8 \times 10^{-9}$ m².

not affect the fact that the relatively short modulation time favors the excitation of extreme pulses.

However, during an experiment, the pump current is smooth and cannot change to a certain value abruptly, which will result in variations in the number of extreme pulses and the intensity of the extreme pulses generated by the current modulation. Therefore, we investigate the effect of smooth current perturbations on the system. Figures 10(a), 10(e), and 10(i) show abrupt current perturbations. Figures 10(c), 10(g), and 10(k) show smooth current perturbations. The average rate of change of the smoothed current is 0.0009 A/ns. The total perturbation time is 23 ns. We find that the output pulse plots of all six time series are the same before the perturbation is applied. There are eight extreme pulses in Fig. 10(b) and six extreme pulses in Fig. 10(d). For the case of current perturbation from 0.03 to 0.021 A, the number of extreme pulses generated by the smooth perturbation is lower, and the intensity of the extreme pulses is lower than those in abrupt current perturbations. There are no extreme pulses in Figs. 10(f) and 10(h). The intensity of the high pulses in Fig. 10(h) is also lower than in Fig. 10(f). But the reduction in the number of extreme pulses, as well as the decrease in the intensity of the pulses due to the smooth current perturbation, is also not absolute; for example, compare Fig. 10(j) with Fig. 10(l). Figure 10(l) has an extreme pulse, but Fig. 10(j) does not. In conjunction with Fig. 8, we conclude that when

exciting extreme pulses by modulating the current, there will be some accidental cases. Sometimes extreme pulses can be excited even when the current modulation amplitude is relatively small, as can be seen by comparing Figs. 10(h) and

TABLE I. Parameters used in Equations (1)–(3).

Parameter	Symbol	Value
Injection efficiency	η	0.64 [28]
Pump current	I_0	0.03 A
Elementary charge	q	1.602×10^{-19} C
Optical confinement factor	Γ_p	0.04 [29]
Group velocity of light	v_g	8.38×10^7 m/s [19]
Spontaneous emission time	τ_{sp}	15 ns [28]
Auger lifetime	τ_{aug}	1.08 ns [28]
Stage number	m	5 [30]
Photon lifetime	τ_p	10.5 ps [19]
Spontaneous emission factor	β	1×10^{-4} [31]
Linewidth enhancement factor	α	2.2 [17]
Cavity length	L	2 mm [30]
Cavity width	W	4.4 μm [30]
Facet reflectivity	R	0.32 [29]
Active area	A	8.8×10^{-9} m ² [32]
Differential gain	a_0	2.8×10^{-10} cm [19]
Transparent carrier number	N_{tr}	6.2×10^7 [32]

10(I). But relatively speaking, the probability of success in exciting extreme pulses is large when the amplitude of the current modulation is large.

IV. CONCLUSIONS

In this work, we simulated the nonlinear dynamics of an ICL under optical injection using rate equations. In particular, this study revealed the dynamic output characteristics of an ICL under optical injection. ICLs with a small stage number and large active area have a relatively large phase-locked region and can generate a large number of P1 oscillations. In the frequency-unlocked region, most of the extreme pulses are concentrated in the region in which the frequency of the slave laser is slightly bigger than the frequency of the master laser. ICLs with a relatively small stage number are more likely to spontaneously generate extreme pulses. An extreme pulse can be triggered or suppressed by step-down current perturbation. Large amplitudes of perturbation currents are more likely to produce extreme pulses with high intensity within the appropriate perturbation time range. Moreover, the generation of extreme pulses is not linked to the time point of the

perturbation. By comparing the effects of smoothly perturbing the pump current and abruptly perturbing the pump current on the extreme pulses, we find that smoothing the perturbing pump current does not absolutely make the number and intensity of extreme pulses decrease. The theoretical scheme proposed in this paper is experimentally feasible. We hope that the present work will advance experimental studies on ICLs under optical injection and provide a different idea about extreme pulse dynamics.

The data that support the findings of this study are available from the corresponding author upon reasonable request.

ACKNOWLEDGMENTS

This work was supported by the National Natural Science Foundation of China (Grants No. 61975225, No. 61927813, No. 12333012, and No. U2241227) and the Science and Technology Commission of Shanghai Municipality (Grant No. 21DZ1101102).

The authors declare no conflict of interest.

-
- [1] C. Lin, R. Q. Yang, D. Zhang, S. J. Murry, S. S. Pei, A. A. Allerman, and S. R. Kurtz, *Electron. Lett.* **33**, 598 (1997).
 - [2] R. Q. Yang, L. Li, and Y. C. Jiang, *Rep. Prog. Phys.* **34**, 169 (2014).
 - [3] J. R. Meyer, W. W. Bewley, C. L. Canedy, C. S. Kim, M. Kim, C. D. Merritt, and I. Vurgaftman, *Photonics* **7**, 75 (2020).
 - [4] R. Q. Yang, *Superlattices Microstruct.* **17**, 77 (1995).
 - [5] J. Faist, F. Capasso, D. L. Sivco, C. Sirtori, A. L. Hutchinson, and A. Y. Cho, *Science* **264**, 553 (1994).
 - [6] N. Horiuchi, *Nat. Photonics* **9**, 481 (2015).
 - [7] C. R. Webster, P. R. Mahaffy, S. K. Atreya, J. E. Moores, G. J. Flesch, C. Malespin, C. P. Mckay, G. Martinez, C. L. Smith, J. M.-Torres, J. G.-Elvira, M.-P. Zorzano, M. H. Wong, M. G. Trainer, A. Steele, D. Archer, B. Sutter, P. J. Coll, C. Freissinet, P.-Y. Meslin *et al.*, *Science* **360**, 1093 (2018).
 - [8] J. Ohtsubo, *Semiconductor Lasers: Stability, Instability, and Chaos* (Springer, Berlin, Heidelberg, 2013).
 - [9] J. Chern, K. Otsuka, and F. Ishiyama, *Opt. Commun.* **96**, 259 (1993).
 - [10] G. H. M. V. Tartwijk and G. P. Agrawal, *Prog. Quantum Electron.* **22**, 43 (1998).
 - [11] C. Lee, T. Yoon, and S. Shin, *Appl. Phys. Lett.* **46**, 95 (1985).
 - [12] V. Kovanisa, A. Gavrielides, T. B. Simpson, and J. M. Liu, *Appl. Phys. Lett.* **67**, 2780 (1995).
 - [13] S. Wiczorek, T. B. Simpson, B. Krauskopf, and D. Lenstra, *Phys. Rev. E* **65**, 045207(R) (2002).
 - [14] C. Bonatto and J. A. C. Gallas, *Phys. Rev. E* **75**, 055204(R) (2007).
 - [15] C. Bonatto and A. Endler, *Phys. Rev. E* **96**, 012216 (2017).
 - [16] K. Otsuka and S. Sudo, *Phys. Rev. E* **104**, 044203 (2021).
 - [17] Y. Deng, B. B. Zhao, and C. Wang, *Appl. Phys. Lett.* **115**, 181101 (2019).
 - [18] Y. Deng and C. Wang, *IEEE J. Quantum Electron.* **56**, 2300109 (2020).
 - [19] H. Han, X. Cheng, Z. Jia, and K. Shore, *Photonics* **8**, 366 (2021).
 - [20] D. R. Solli, C. Ropers, P. Koonath, and B. Jalali, *Nature (London)* **450**, 1054 (2007).
 - [21] S. N. Chowdhury, A. Ray, S. K. Dana, and D. Ghosh, *Phys. Rep.* **966**, 1 (2022).
 - [22] C. Bonatto, M. Feyereisen, S. Barland, M. Giudici, C. Masoller, J. R. Rios Leite, and J. R. Tredicce, *Phys. Rev. Lett.* **107**, 053901 (2011).
 - [23] J. Zamora-Munt, B. Garbin, S. Barland, M. Giudici, J. R. Rios Leite, C. Masoller, and J. R. Tredicce, *Phys. Rev. A* **87**, 035802 (2013).
 - [24] O. Spitz, J. Wu, A. Herdt, G. Maisons, M. Carras, W. Elsäßer, C.-W. Wong, and F. Grillot, *Adv. Photonics* **2**, 066001 (2020).
 - [25] J. Tian, S. Chen, and M. Cristina, *Opt. Express* **25**, 31326 (2017).
 - [26] R. Lang, *IEEE J. Quantum Electron.* **18**, 976 (1982).
 - [27] X. Wang, B. Zhao, F. Grillot, and C. Wang, *Opt. Express* **26**, 15167 (2018).
 - [28] W. W. Bewley, J. R. Lindle, C. S. Kim, M. Kim, C. L. Canedy, I. Vurgaftman, and J. R. Meyer, *Appl. Phys. Lett.* **93**, 041118 (2008).
 - [29] I. Vurgaftman, W. W. Bewley, C. L. Canedy, C. S. Kim, M. Kim, J. R. Lindle, C. D. Merritt, J. Abell, and J. R. Meyer, *IEEE J. Sel. Top. Quantum Electron.* **17**, 1435 (2011).
 - [30] I. Vurgaftman, C. L. Canedy, C. S. Kim, M. Kim, W. W. Bewley, J. R. Lindle, J. Abell, and J. R. Meyer, *New J. Phys.* **11**, 125015 (2009).
 - [31] L. A. Coldren, S. W. Corzine, and M. L. Masanovic, *Diode Lasers and Photonic Integrated Circuits* (Wiley, Hoboken, NJ, 2012).
 - [32] R. Q. Yang, *Microelectron. J.* **30**, 1043 (1999).
 - [33] C. Wang, F. Grillot, V. Kovanis, and J. Even, *J. Appl. Phys.* **113**, 063104 (2013).
 - [34] W. T. Prants and C. Bonatto, *Phys. Rev. E* **103**, 032201 (2021).
 - [35] S. C. Chan, S. K. Hwang, and J. M. Liu, *Opt. Express* **15**, 14921 (2007).